Coherency Strain and Dislocations in Copper-Rich-Precipitate Embrittled A710 Ferritic Steels

Davor Balzar

Metallurgical and Materials Transactions A

ISSN 1073-5623
Volume 43
Number 5

Metall and Mat Trans A (2012)
43:1462-1467
DOI 10.1007/s11661-011-0827-4

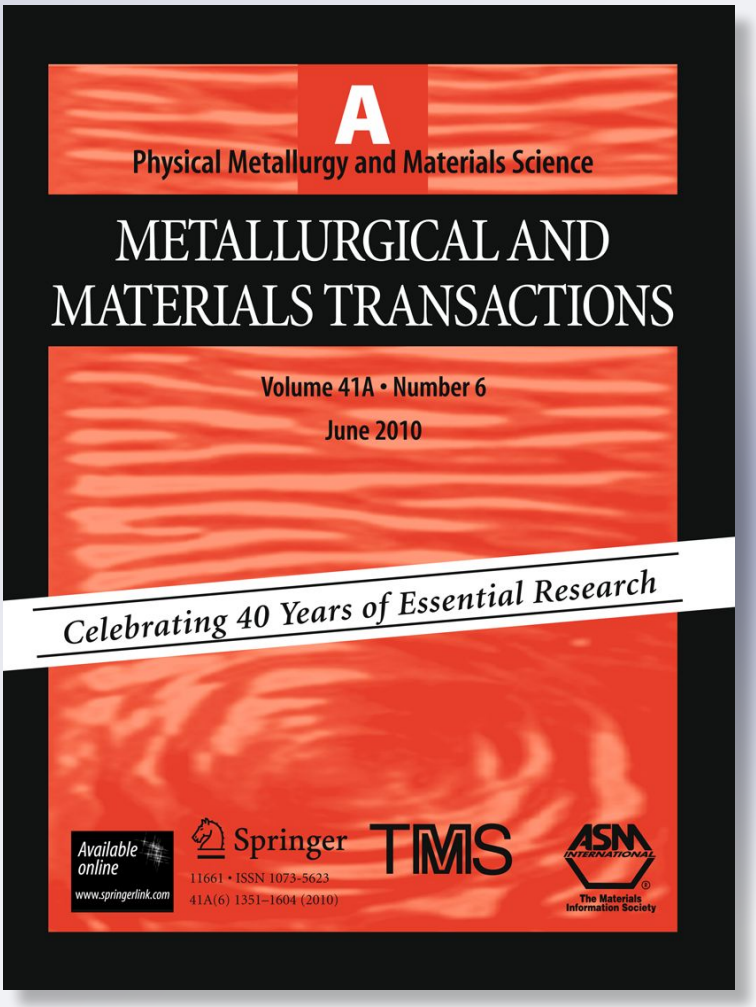

Springer

Coherency Strain and Dislocations in Copper-Rich-Precipitate Embrittled A710 Ferritic Steels

DAVOR BALZAR

The irradiation embrittlement of reactor pressure vessel steels was studied on surrogate samples of A710 ferritic steels, which is rich in copper. Dislocations and coherency strain caused by the copper-rich precipitates, as a function of aging time, were studied by small-angle neutron scattering, diffraction line-broadening analysis, transmission electron microscopy, and Eshelby inclusion method. Aging has induced copper-rich precipitate nucleation and growth, thus impeding the dislocation motion and hardening the steels. The precipitates are coherent with the matrix up to about 3.5 nm in radius, when they become semi coherent with the ferritic matrix, thus relaxing strains/stresses and softening it. There is good agreement between all experimental techniques used and the Eshelby inclusion model.

DOI: 10.1007/s11661-011-0827-4

I. INTRODUCTION

RADIATION-INDUCED embrittlement of nuclear reactor pressure vessel (RPV) steels is a long-standing issue for safety of nuclear power plants. Because of the resurgent interest in nuclear power plants, the International Atomic Energy Agency (IAEA) has recently published a comprehensive technical report on assessment of irradiation-embrittlement effects on RPV steels.[1] The embrittlement mainly occurs because of the impeded dislocation motion. Dislocations are pinned by different obstacles: Diffusion rates in the ferrite matrix are substantially enlarged by defects created by irradiation; clusters and later precipitates are formed. The copper-rich precipitates (CRPs) in steels that are rich in copper are extremely important in causing the embrittlement. In steels with the copper content below 0.1 mass pct, manganese-nickel rich (MNR) precipitates can form. In both cases, precipitates contain significant amounts of iron and other elements, such as silicon. Phosphorus has been known to also have a serious deleterious effect.[1] It is not clear, however, how much importance other matrix defects play, such as displacement cascade vacancy-solute clusters or nanovoids. To study the effects of CRP separately, it is therefore necessary to resort to surrogate systems. This study is based on the surrogate samples made for a comprehensive effort to characterize the embrittlement by nondestructive methods.[2] Here, we describe the small-angle neutron scattering (SANS) and line-broadening analysis (LBA) results in more detail, which, together with a simple coherency strain model and dislocation densities, complements the interpretation of the embrittlement mechanism.

DAVOR BALZAR, Associate Professor, is with the Department of Physics and Astronomy, University of Denver, 2112 E. Wesley Ave, Denver, CO 80208. Contact e-mail: balzar@du.edu
Manuscript submitted April 15, 2011.
Article published online July 20, 2011

II. EXPERIMENTAL

We used a commercially available ASTM classification A710 steel. This steel has a low carbon (0.05 mass pct) and high copper content (1.13 mass pct), in order to facilitate as much as possible formation of copper-rich over carbide precipitates. The specimens were initially solution treated at 1173 K (900 °C) and furnace cooled to ambient temperature. Then a series of specimens was prepared by aging at 723 K (450 °C) for different times[2] and cooled in perlite to ambient temperature. This thermal treatment was expected to produce precipitates with different size and distribution. Hardness measurements were used to indicate the onset of incoherence with the matrix. Specimens for the SANS measurements were cut out of the larger pieces in approximate size of 20 × 20 × 2.3 mm.

The SANS measurements were collected with the NG-7 30 m instrument at the NIST Center for Neutron Research (NCNR). NG-7 uses cold neutrons moderated with liquid hydrogen at 20 K (–253 °C) with an available neutron wavelength in the range 0.5 – 2 nm. The sample-to-detector distance can be continuously varied from 1 to 15 m. The total Q ($Q = 4\pi \sin\theta/\lambda$), where 2θ is the scattering angle) range, extends from 0.015 to 6 nm^{-1}; that is, the approximate size regime is 0.5 – 200 nm. The detailed description of the instrument can be found elsewhere.[3]

Specimens were mounted in the specimen changer with a large surface normal to the beam direction. During the measurements, a magnetic field of 1.8 T induction was applied in a horizontal plane, perpendicular to the neutron-beam direction, to suppress magnetic domain-wall scattering. The sample-detector distances used were 1, 8, and 14 m. The wavelength used was 1 nm, and the measurements were collected with a rectangular (640 mm square) position-sensitive He-3 proportional counter with 1-cm^2 spatial resolution.

Raw measurements were corrected by empirical detector efficiency correction factors obtained by the

measured scattering from a plexiglass sample. Data were then normalized to a fixed number of incident neutrons and corrected for background and empty cell scattering. Correction for the sample transmission was determined by measuring the attenuated direct beam and scaling to the value of the empty sample holder. Finally, the data were put on the absolute scale by normalizing to the standard sample of polystyrene.

X-ray-diffraction data were collected using a Scintag V θ-2θ powder diffractometer with vertical axis, 22 cm radius, at 45 kV and 40 mA. $Cu_{K\alpha}$ radiation was collimated with Soller slits and a 2-mm divergence slit. Soller slits in the diffracted beam, 0.2-mm receiving slit and Ge solid-state detector, were used in a step-scanning mode (0.01°/10 s in the 2θ region 18° – 78° and 0.02°/30 s in the 2θ region 78° – 155° for standard specimen, 0.02°/50 s in the 2θ region 35° – 145° for steel specimens).

III. RESULTS AND DISCUSSION

A. *SANS*

In a simple two-phase model, the scattering cross section Σ per solid angle Ω is calculated as:

$$\frac{d\Sigma}{d\Omega} = (\eta_p - \eta_m)^2 f_V V_p |F(Q)|^2 \qquad [1]$$

Here, subscript p relates to precipitate (particle) and m to matrix, η is a scattering-length density, f_V volume fraction, V volume, and F a scattering function (form factor).

Because of a horizontal external magnetic field, the horizontal component of the scattering cross section contains the nuclear component only. The ratio between vertical and horizontal component M is then given by contrast in nuclear $\Delta\eta_{nuc}$ and magnetic $\Delta\eta_{mag}$ scattering-length densities:

$$M = \frac{(d\Sigma/d\Omega)_\perp}{(d\Sigma/d\Omega)_\parallel} = \frac{\Delta\eta_{nuc}^2 + \Delta\eta_{mag}^2}{\Delta\eta_{nuc}^2} \qquad [2]$$

We take $\eta_{nuc} = 8.0852 \cdot 10^{10}/cm^2$ and $\eta_{mag} = 5.31 \cdot 10^{10}/cm^2$ for steel and $\eta_{nuc} = 6.5530 \cdot 10^{10}/cm^2$ for precipitates; that is, we assume pure iron and copper compositions, respectively. The ratio M hence depends on the composition of the matrix and precipitates. For instance, for pure Cu precipitates in Fe matrix, $M = 13$, and for vacancies in Fe, $M = 1.4$. One could potentially estimate precipitate compositions based on the measured M ratio.[4] The ratio M for our specimens varied in a relatively large range from 2.3 (CC-6 and CC-7) to 4.8 (CC-4). Furthermore, the trend indicated that the Mn content increases as precipitates grow, which is contrary to the expected; that is, the precipitates are on growth expected to become more copper-rich. Because precipitates can contain significant amounts of Fe, especially in the early precipitation stages, we did not attempt to estimate the composition of precipitates.

The scattering cross sections, as determined from the measurements taken at the 14-m detector-sample distance, on an absolute scale of all seven specimens are shown in Figure 1(a). It is evident that only the nontreated specimen CC-1 shows a distinct distribution of scatterers of the larger size; this may be attributed to some retained austenite that is dissolved even after a short aging time of 10 min for the specimen CC-2. Therefore, we excluded the CC-1 specimen from the subsequent analysis. Figure 1(b) shows the same data for the 1-m detector-sample distance, where large changes occur in the size range 3 – 5 nm. Scattering cross-section curves on the absolute scale for specimens CC-3 to CC-7 were corrected with the scattering cross-section curves for CC-2, and all the reported results are relative to the CC-2 specimen.

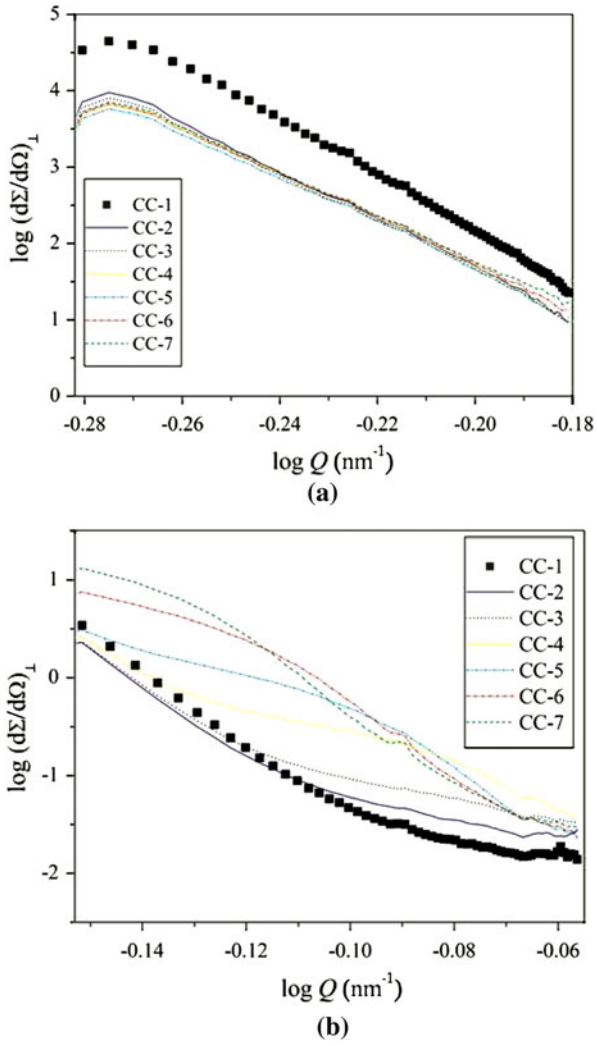

Fig. 1—The scattering cross section Σ per solid angle Ω as a function of the wavevector Q ($Q = 4\pi \sin\theta/\lambda$, where 2θ is the scattering angle): (*a*) 14-m detector-sample distance and (*b*) 1-m detector-sample distance.

In the analysis of the difference scattering curves, we make two assumptions: Precipitates are of spherical shape, and they are distributed according to a log-normal distribution.[4] The shape is likely to be governed by elastic properties; that is, if precipitates are softer than the matrix, they would assume an elongated,

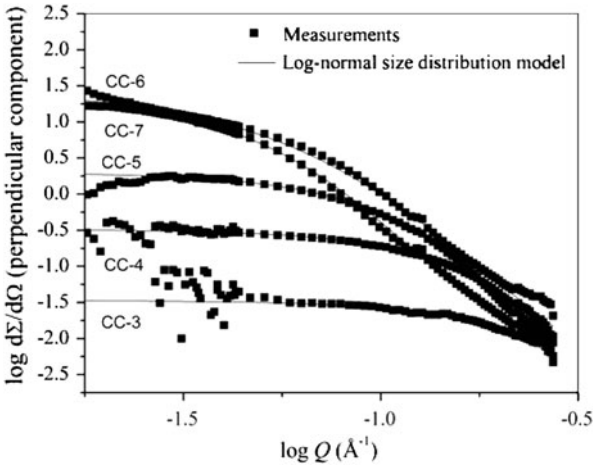

Fig. 2—Fits to the experimental data on the assumption of log-normal size distribution of spherical scatterers.

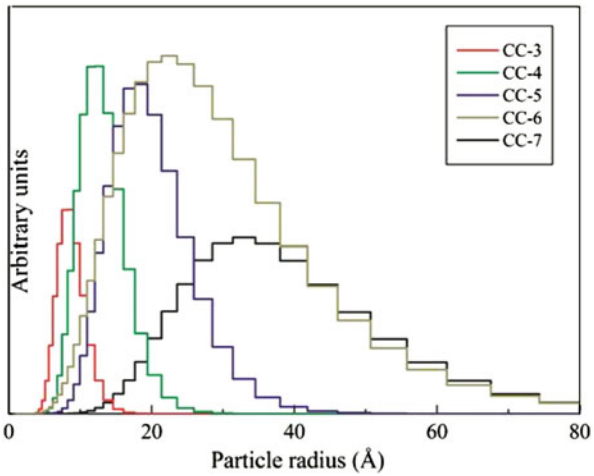

Fig. 3—Particle size distributions on the assumption of log-normal size distribution of spherical scatterers.

disc-like shape.[5] However, when precipitates are very small, there is a tendency to a spherical shape because of a surface tension. In either case, the spherical shape may be a satisfactory first-order approximation.

Hence:

$$F(Q) = 3\frac{\sin(QR) - QR\cos(QR)}{(QR)^3} \qquad [3]$$

$$N(R) = \frac{N}{\sqrt{2\pi}\beta R}\exp\left\{-\frac{1}{2}\left[\frac{\ln(R/R_m)}{\beta}\right]^2\right\} \qquad [4]$$

Here, N is a precipitate number density, R is a precipitate radius, R_m is a distribution maximum (mode), and β is its width parameter. Figure 2 presents fits to the difference scattering curves, and Figure 3 shows the resulting size distributions. The distribution maximum shifts toward the larger sizes, and there is an overall effect of distribution broadening, which indicates that copper is continuously extracted from the solution. Figure 4 presents changes in particle radius, number density, and volume fraction, where we assumed:

$$f_V = N\bar{V}_p = \frac{4\pi}{3}N\overline{R^3} \qquad [5]$$

The particle radius increases approximately linearly with the logarithm of aging time and extrapolates to zero radius for the sample CC-2, which was used as a reference sample. There is a maximum in volume fraction for specimen CC-6, after which the volume fraction decreases. This seems to indicate that all the copper is precipitated out of the matrix in the specimen CC-6, after which some copper gets dissolved back into the matrix as a result of a prolonged aging.

B. *X-Ray Diffraction Line-Broadening Analysis*

Small copper-rich precipitates are coherent with the α-Fe matrix. This results in an inhomogeneous coherency strain of the host crystal lattice. The effect is similar to a distortion of a regular crystal lattice by point defects or dislocations and is discernible by diffraction line-broadening measurements.[6] To obtain the values of an inhomogeneous strain, the so-called "double-Voigt" model for size-strain analysis was used.[7] Diffraction line widths were corrected for instrumental line broadening, by measuring the broadening of an NIST SRM660a LaB_6, and the subsequent line-broadening analysis yielded the mean-square strain.[8] The magnitude of strain for the A710-alloy series is in the range $5.3 - 6.9 \cdot 10^{-4}$ and directly correlates with Rockwell hardness as shown in Figure 5. Because hardness depends on the internal stress required to move dislocations in the host lattice, it is dependent on the coherency state of the precipitates: For as-quenched steel, small copper-rich precipitates already form. Their coherency strains pin dislocations and thus inhibit their motion. In the aged steel, coherent precipitates are of optimum size and strain the matrix maximally (CC-6). On overaging, the precipitates grow larger than the critical size and become incoherent (or semicoherent) with the matrix. This largely relieves the coherency strain, the dislocations can move more easily, and the hardness decreases (cf. CC-7).

C. *Coherency Strain and Inclusion Method*

In the Eshelby inclusion method,[9,10] an inclusion of a misfit ε, defined by the initial radius of the inclusion R_0^* and the radius of the hole in the matrix R_0, will cause strain e in the matrix:

$$e_{rr} = -2C\varepsilon(R_0/r)^3;\ e_{\theta\theta} = e_{\varphi\varphi} = C\varepsilon(R_0/r)^3;\ r \geq R_0 \qquad [6]$$

$$\varepsilon = R_0^*/R_0 - 1;\ C = 3B^*/(3B^* + 4G) \qquad [7]$$

Here, B and G are bulk and shear moduli, respectively.

Inhomogeneous strain will be manifested by line broadening of the matrix diffraction lines. From the elastic energy considerations, one can estimate the

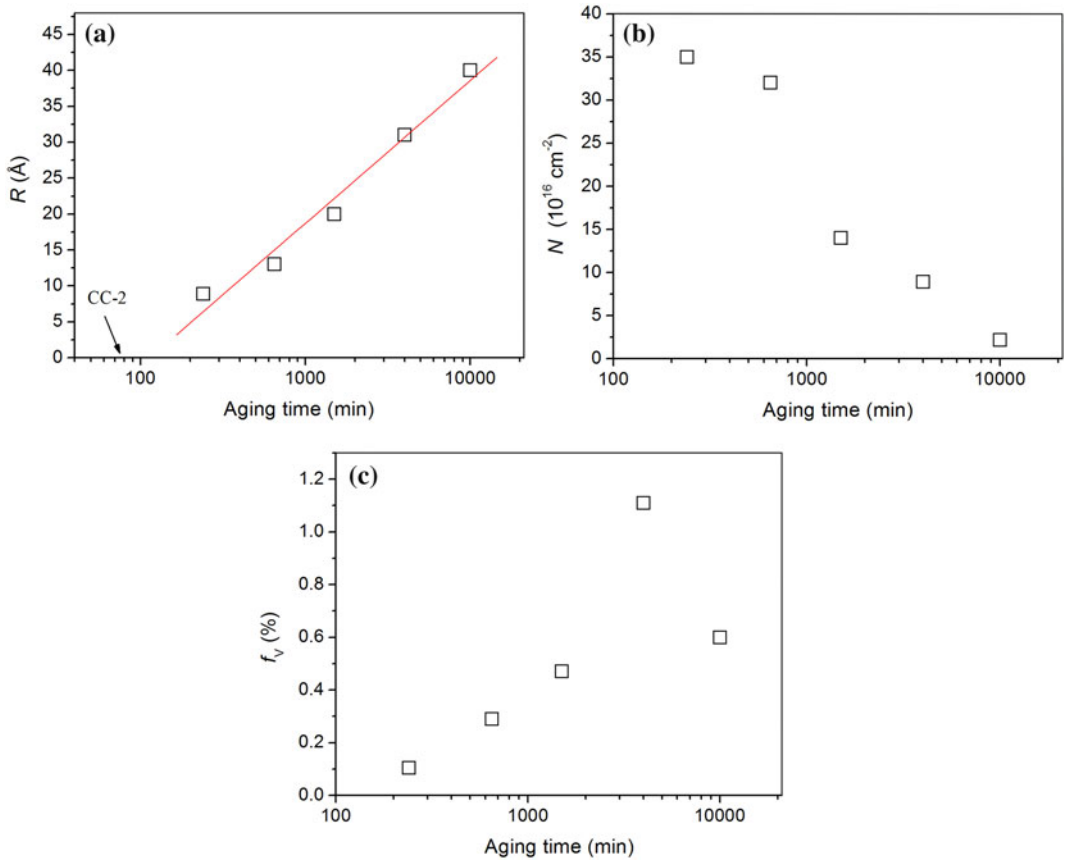

Fig. 4—(*a*) Particle radius (*b*) number density; and (*c*) volume fraction as a function of aging time.

following relationship between the root-mean-square strain and CRP volume fraction:

$$\langle e^2 \rangle^{1/2} = \frac{2}{\sqrt{5}} C \frac{\varepsilon}{(1+\varepsilon)^3} f_V^{1/2} \quad [8]$$

Figure 6 shows the plot. As expected, CC-7 does not follow the trend because in this overaged sample the precipitates are incoherent with the matrix.

By extrapolating to the zero CRP volume fraction in Figure 6, one gets a residual strain of about $5\ 10^{-4}$. This strain is caused by dislocations that are present in all samples. One can estimate the density of dislocations by using[11] :

$$\rho = \frac{k}{F} \frac{\langle e^2 \rangle}{b^2} = 6 \cdot 10^9 / \mathrm{cm}^2 \quad [9]$$

The TEM results[12] confirm the order of magnitude for the dislocation density. This relatively high density of dislocations can be understood in the view of the published theoretical model,[13] which confirmed an onset of a semicoherent twinned precipitate at a critical size, accompanied by creation of misfit dislocations and a release of additional dislocations into the matrix. This introduction of misfit dislocations should at least partially relieve the coherency strain and thus facilitate lattice-dislocation mobility. Consequently, lattice dislocations might be able to achieve energetically more stable arrangements and therefore lower the overall elastic energy. According to our SANS results (compare Figure 4), this transformation occurs when CRP reach the radius of about 35 Å (3.5 nm), which agrees well with the published TEM results.[14]

If the calculated Eshelby strain caused by CRP (Eq. [8]), an estimate of strain from TEM measurements[12] caused by dislocations (Eq. [9]), and root-mean-square strain, as determined by diffraction line-broadening analysis (Figure 5), are all considered, there is a very good qualitative and quantitative agreement (Figure 7). This indicates that a simple inclusion model, along with SANS, LBA, and TEM, gives a coherent physical picture about the hardening and embrittlement mechanism by CRP in these ferritic steels.

IV. CONCLUSIONS

In summary, it has been shown that copper-rich precipitates form upon aging of the copper-rich ferritic A710 steels. These precipitates strain the ferritic matrix and thus impede motion of dislocations, causing hardening. The precipitate size distributions, number densities, and volume fractions were determined by SANS. The inhomogeneous strains emanating from diffraction line broadening were also measured. These strains have contributions from Eshelby coherency strains caused by

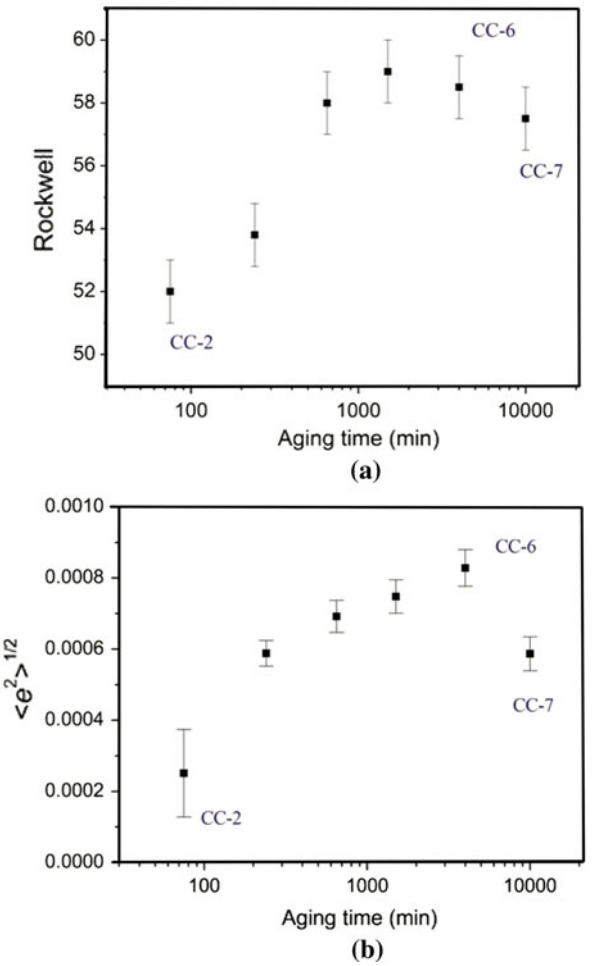

Fig. 5—Rockwell A hardness (*a*) and root-mean-square strain determined from diffraction line broadening (*b*), as a function of aging time.

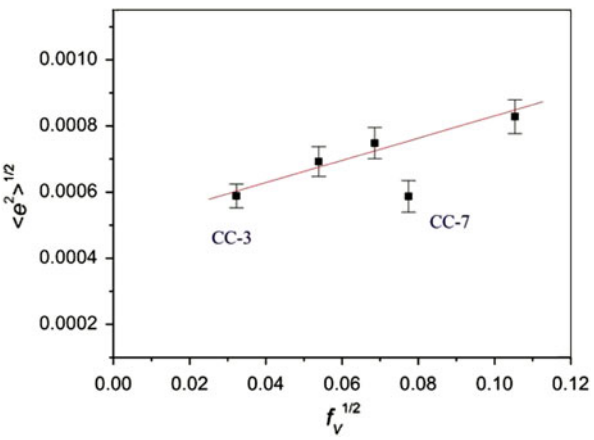

Fig. 6—Root-mean-square strain determined from diffraction line broadening as a function of the square root of the particle volume fraction, following Eq. [8].

inhomogeneous inclusions (precipitates) and lattice dislocations. Upon prolonged aging, precipitates become semicoherent with the matrix (at about 3.5 nm in radius), which relieves the strain. As a result, dislocations can move more freely, which is likely to decrease their density and steel hardness. The absolute value of the inhomogeneous strain is in a good agreement with the calculated Eshelby strain and dislocation densities that were estimated by TEM.

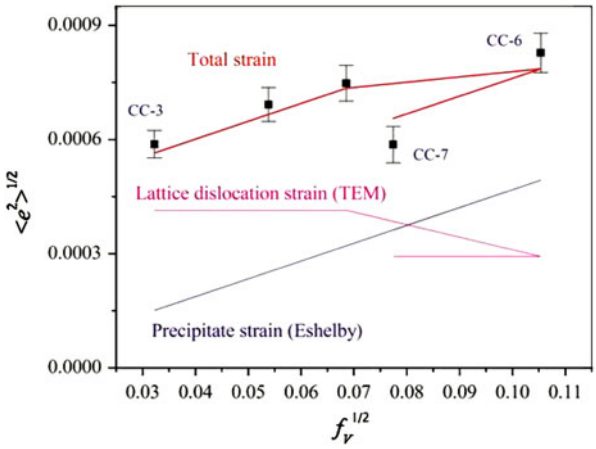

Fig. 7—The calculated coherency strain from precipitates (Eshelby model) and strain from the lattice dislocations (as estimated from dislocation densities measured by TEM on the assumption that the dislocation density does not appreciably change for CC-3, CC-4, and CC-5) add to a total strain (full red line). Root-mean-square strain from diffraction line broadening is also plotted (full squares).

ACKNOWLEDGMENTS

The author is indebted to H. Ledbetter, G. Alers, D. Hurley, B. Igarashi, W. Johnson, S. Kim, D. McColskey, and P. Purtscher for helpful discussions. H. Ogi (University of Osaka, Japan) has provided TEM measurements. The NG-7 SANS beamline at the NIST Center for Neutron Research and instrument scientists are gratefully acknowledged. The author thanks Günter Goerigk (Helmholtz-Zentrum Berlin für Materialien und Energie) for very helpful comments, especially regarding SANS measurements and data analysis.

REFERENCES

1. "Integrity of Reactor Pressure Vessels in Nuclear Power Plants: Assessment of Irradiation Embrittlement Effects in Reactor Pressure Vessel Steels", IAEA Nuclear Energy Series Technical Reports No. NP-T-3.11, International Atomic Energy Agency, Vienna, 2009.
2. G. Alers, D. Balzar, D.C. Hurley, B. Igarashi, F. Fickett, S. Kim, H. Ledbetter, and P. Purtscher: *Proc. 9th Int. Symp. on Nondestructive Characterization of Materials IX*, AIP Conference Proceedings 497, Ed. R.E. Green, American Institute of Physics, Melville, New York, 1999, pp. 419–24.
3. C.J. Glinka, J.G. Barker, B. Hammouda, S. Krueger, J.J. Moyer, and W.J. Orts: *J. Appl. Cryst.*, 1998, vol. 31, pp. 430–45.
4. B.D. Wirth, G.R. Odette, W.A. Pavinich, G.E. Lucas, and S.E. Spooner: *Proc. Effects of Radiation on Materials: 18th International Symposium,* A S T M S T P 1325, Eds. R.K. Nanstad,

M.L. Hamilton, F.A. Garner, and A.S. Kumar, West Conshohocken, PA, 1999, p. 102.
5. J.K. Lee: *Metall. Mater. Trans. A*, 1996, vol. 27A, pp. 1449–59.
6. V. Hauk: *Structural and Residual Stress Analysis by Nondestructive Methods*, Elsevier, Amsterdam, the Netherlands, 1997, p. 216.
7. D. Balzar and H. Ledbetter: *J. Appl. Cryst.*, 1993, vol. 26, pp. 97–103.
8. D. Balzar: *Microstructure Analysis from Diffraction*, Eds. R.L. Snyder, H.J. Bunge, and J. Fiala, International Union of Crystallography, Chester, UK, 1998, pp. 94–126.
9. J.D. Eshelby: *Proc. Roy. Soc. London A*, 1957, vol. 241, p. 376.
10. T. Mori and K. Tanaka: *Acta Metall.*, 1973, vol. 21, pp. 571–74.
11. G.K. Williamson and R.E. Smallman: *Phil. Mag.*, 1956, vol. 1, pp. 34–46.
12. H. Ogi: Private communication, 1998.
13. J.K. Lee: *Metall. Mater. Trans. A*, 1998, vol. 29A, pp. 2039–48.
14. I. Altpeter, G. Dobmann, K.-H. Katerbau, M. Schick, P. Binkele, P. Kizler, and S. Schmauder: *Nucl. Eng. Des.*, 2001, vol. 206, pp. 337–50.